JOURNAL OF AIRCRAFT
Vol. 44, No. 3, May–June 2007

Aerodynamic Performance Analysis of a Gurney Flap for Rotorcraft Application

Kwanjung Yee*
Pusan National University, Busan 609-735, Republic of Korea
Wandon Joo†
Doosan Heavy Industries and Construction, Daejeon 305-348, Republic of Korea
and
Dong-Ho Lee‡
Seoul National University, Seoul 151-742, Republic of Korea

DOI: 10.2514/1.26868

In the present study, the aerodynamic characteristics of the Gurney flap were comprehensively investigated in terms of the performance requirements for a helicopter rotor by using two-dimensional Navier–Stokes equations. To this end, with the rotor operating flow conditions in mind, the static aerodynamic characteristics of the Gurney flap are thoroughly compared with those of the clean airfoil at various Mach numbers, incidences, and Gurney flap heights. Next, to understand the general dynamic stall features of the airfoils with the Gurney flap, a series of parametric studies are performed with respect to oscillating frequency and amplitude, and the correlations of the aerodynamic coefficients are obtained by using the dynamic stall function of Bousman. It is concluded that there exists some optimum Gurney flap heights, which minimize the drag and pitching moment while maximizing the lift coefficient and lift-to-drag ratio at the same time. In the present study, the 2% Gurney flap would be a good compromise to satisfy all the major rotorcraft design criteria.

Nomenclature

a_∞	=	speed of sound
a_i, b_i	=	polynomial coefficients for $Cl_{\max}$, $i = 0, 1, 2$
C	=	airfoil chord
Cd	=	drag coefficient
Cd_0	=	drag coefficient at zero-lift
$Cd_{\max}$	=	maximum drag coefficient
Cl	=	lift coefficient
$Cl_{\max}$	=	maximum lift coefficient
Cm	=	moment coefficient
Cm_0	=	moment coefficient at zero-lift
$Cm_{\min}$	=	minimum moment coefficient
$\boldsymbol{E}$, $\boldsymbol{F}$	=	convective fluxes
$\boldsymbol{E}_v$, $\boldsymbol{F}_v$	=	viscous fluxes
J	=	Jacobian of transformation matrix
k	=	$\omega/2M_\infty$, reduced frequency of oscillating airfoil motion
L/D	=	lift-to-drag ratio
M_{DD}	=	zero-lift drag divergence Mach number
M_∞	=	freestream Mach number
$\boldsymbol{Q}$	=	vector of conservative variables
t	=	nondimensionalized physical time
t_c	=	nondimensionalized computational time
x, y	=	Cartesian coordinate
α	=	angle of attack
ξ, η	=	time-dependent curvilinear coordinates
ρ_∞	=	freestream density
ω	=	frequency of oscillating airfoil motion, rad/s

Received 29 July 2006; revision received 25 November 2006; accepted for publication 25 November 2006.

*Assistant Professor, Department of Aerospace Engineering, San 30, Jangjeon-Dong, GeumGeong-gu; daedalus@pusan.ac.kr. AIAA Member.
†Senior Researcher, Corporate Research and Development Institute, 58-4 Hwaam-dong, Yuseong-gu; wandon.joo@doosan.com. AIAA Member.
‡Professor, School of Mechanical and Aerospace Engineering, BD 301-1302, San 56-1, Shinlim-dong, Gwanak-gu; donghlee@snu.ac.kr. AIAA Member.

Introduction

THE previous research of the Gurney flap is focused on lift-enhancement mechanisms and application on performance enhancement devices for fixed wing aircraft. Recently, a great amount of the research is conducted on various applications of the Gurney flap. However, research on the Gurney flap focused on the design of helicopter rotor blades is rare. Therefore, a performance and limitation of the Gurney flap was tried to investigate from the viewpoint of rotorcraft application. To this end, numerical experiments were performed about Gurney flap length from 0.5 to 4.0% chord for various Mach numbers and angles of attack, and the results were assessed.

The Gurney flap is a small strip located on the trailing edge of the airfoil on the pressure side, perpendicular to the mean chord line. It is named after the car racer Daniel Gurney who first used the Gurney flap to increase the down force and stability of the car at high-speed cornering. In spite of its mechanical simplicity, it is well known to bring a remarkable improvement of the maximum lift coefficient of the airfoil with only a small change of stall angle [1].

Significant lift-enhancement capability of the Gurney flap has a great potential for the application to the helicopter rotor blade design because it can be a useful tool to alleviate dynamic stall and improve the aerodynamic performance of airfoil at dynamic stall, which typically occurs in the high-speed forward flight of the helicopter. Hence, once the aerodynamic effectiveness of the Gurney flap is validated under the actual operating conditions of the helicopter rotors, the performance increase of the rotor blades can be obtained through a simple modification of rotor design. The airfoil with improved lift has a great impact on the overall rotor performance because it may reduce rotor blade areas and rotor system weight. In addition, for the same blade area, it may increase aircraft gross weight, speed, or altitude capability. Alternatively, it may help reduce tip speed without loss of the thrust as the noise requirements become severe.

The Gurney flap is not a novel concept. Actually, it has been extensively studied since the 1960s. However, the research accomplished so far mainly focused on the elucidation of the lift-enhancement mechanism of the Gurney flap. Liebeck [2] suggested that there existed a short separation region of the upstream of the Gurney flap and the counter-rotating vortices in the downstream. Through the flow visualization of a Newman airfoil with 1.5% chord Gurney flap using tuft, he also observed that the wake in the downstream of the Gurney flap turned locally due to these vortices. Neuhart and Pendergraft found similar vortical flow structures around the NACA 0012 airfoil with Gurney flap in the water tunnel at a relatively low Reynolds number ($Re = 8.6 \times 10^3$) [3]. At this Reynolds number, it was difficult to identify any flow instabilities caused by the Gurney flap.

In Jang and Ross's numerical study using Reynolds-averaged Navier–Stokes simulation, it was noticed that the Gurney flap shifted the location of the Kutta condition and the resulting wake-turning effect alleviated the adverse pressure gradient at the trailing-edge region, and thereby increased the suction over the suction side [4].

Storms and Jang measured the aerodynamic loading and pressure distribution of the NACA 4412 airfoil by attaching a Gurney flap and vortex generator, and showed that the Gurney flap had a tendency to produce additional nose-down pitching moment [5].

Myose et al. conducted a wind tunnel experiment in a low-speed wind tunnel. A symmetric NACA 0011 airfoil and a cambered GA (W)-2 airfoil were used for single-element airfoil. For a two-element airfoil, a GA(W)-2 airfoil was used and an NLF airfoil was used for a three-dimensional wing. It was observed that the drag increase was inevitable when using the Gurney flap [6]. In addition, a slight improvement in performance was observed when the Gurney flap was located inboard rather than outboard of a three-dimensional wing. It was also confirmed that a downward turning of the wake after the Gurney flap resulted in the increase of effective camber of the airfoil. Van Dam et al. [7] investigated the effect of both solid and serrated Gurney flaps and compared the results with Myose's experiments [6]. The results showed good agreement in terms of the Gurney flap's overall effect on the lift characteristics of wings. However, it was observed that it is not always effective on a three-dimensional configuration when the Gurney flaps extended along with the span. Rather, spanwise variation in the flap geometry, such as serrations, allowed the modulation of lift increment without severe drag penalties.

Giguère et al. conducted an experimental study of scaling of the Gurney flap for optimum lift-to-drag ratio. With a modified LA203A airfoil in a low-speed wind tunnel test, it was suggested that the drag increase could be minimized when the Gurney flap was located within the boundary layer [8].

Jeffrey et al. conducted the experiment to measure the airfoil surface pressure and velocity field by using laser Doppler velocimetry [9]. It was observed that the wake downstream of the Gurney flap consisted of the Karman vortex streets of alternating vortices. The alternating vortices were consistently shed from the Gurney flap, which lowered the pressure of downstream side of the Gurney flap while increasing the pressure of the pressure side. Consequently, it was concluded that this pressure difference acted on both sides of the Gurney flap and increased the circulation and lift.

From the preceding research mentioned, it seems that the overall mechanism of the lift increase by the Gurney flap is generally understood. Nonetheless, because the previous research mainly relied on the wind tunnel experiment at subsonic speed, there are only a few publications available which focused on the aerodynamic and aeroelastic characteristics of the Gurney flap at the higher Mach number region. Moreover, few researches were conducted on the unsteady aerodynamic characteristics of the Gurney flap, which is the key to the application of Gurney flap to the rotating blades, such as helicopter rotor blades and wind turbines.

Recently, Chandrasekhara et al. [10] suggested that to resolve the drawback of the Gurney flap, such as the increase in moment and drag, variable droop leading edge and Gurney flap were applied. As a result, the lift, moment, and drag characteristics of a VR-12 airfoil were improved simultaneously. Despite the remarkable result, this method has some disadvantages. Variable droop leading edge requires additional power as well as additional space to install actuator systems. Joo et al. [11] showed that the optimized combination of fixed leading-edge droop and Gurney flap performed similarly with the combined variable leading-edge droop and Gurney flap.

Maughmer et al. [12] conducted various researches on active Gurney flap named miniature trailing-edge effectors. It was shown that a miniature trailing-edge effector (MiTE) could improve rotor performance by a 20% increase in maximum flight speed, a 16% increase in the maximum lift-to-drag ratio, and a 10% increase in potential thrust by the performance analysis based on the blade element momentum theory (BEMT).

In addition, Yeo [13] conducted a comparative study of seven active control concepts when they are applied to a four blade rotor with VR-12 airfoil by using CAMRAD II. He found that individual blade control, active twist, and trailing-edge flap concepts improved the rotor lift-to-drag ratio with 2/revolution harmonic control. And leading-edge slat, variable droop leading edge, oscillatory jet, and Gurney flap increased the blade maximum loading capability when the devices were used over the retreating side of the rotor disk. His research shows that the Gurney flap can be a competitive control concept for helicopter rotor blades.

Despite the many previous impressive works, comprehensive aerodynamic studies for the Gurney flap airfoil are seldom found from the viewpoint of rotor blade design. Therefore, it is worthwhile to investigate both steady and unsteady aerodynamic characteristics of the Gurney flap retaining the viewpoint of helicopter rotor blade performance enhancement and limitation of its application. Especially, the unsteady aerodynamics related with the dynamic stall is of particular interest because the flight limit and performance will be restricted by dynamic stall.

To this end, with the rotor operating flow conditions in mind, the static aerodynamic characteristics of the Gurney flap were thoroughly compared with those of the clean airfoil at various Mach numbers, incidences, and Gurney flap heights.

Next, to understand the general dynamic stall features of the airfoils with the Gurney flap, a series of parametric studies were performed with respect to oscillating frequency and amplitude, and the correlations of the aerodynamic coefficients were obtained by using the dynamic stall function of Bousman [19,20,23].

Governing Equations and Numerical Approach

Two-dimensional unsteady Reynolds-averaged Navier–Stokes equations are used for this study. By introducing the general curvilinear coordinate system $\xi = \xi(t, x, y)$ and $\eta = \eta(t, x, y)$, the governing equations are written in conservative form.

$$\frac{1}{J}\frac{\partial \boldsymbol{Q}}{\partial t_c} + \frac{\partial \boldsymbol{E}}{\partial \xi} + \frac{\partial \boldsymbol{F}}{\partial \eta} = \frac{\partial \boldsymbol{E}_v}{\partial \xi} + \frac{\partial \boldsymbol{F}_v}{\partial \eta} - \frac{1}{J}\frac{\partial \boldsymbol{Q}}{\partial t} \tag{1}$$

In Eq. (1), $\boldsymbol{Q}$ represents $[\rho, \rho u, \rho v, \rho e, k, \omega]^T$ in a two-dimensional problem, and $J = \xi_x \eta_y - h_x \xi_y$. All geometric variables are nondimensionalized by airfoil chord length, density by freestream density, and velocity u, v by speed of sound, separately.

A dual time-stepping method was used to obtain higher order temporal accuracy for unsteady flowfields. Roe's flux difference scheme is used for spatial discretization of inviscid terms, whereas a central difference scheme is reserved for discretization of viscous terms. Computation time has been greatly reduced through parallel computing for which the data-parallel symmetric Gauss–Seidel (DP-SGS) [14] method and domain decomposition method are employed. DP-SGS uses pointwise symmetric Gauss–Seidel sweep in the interior of subdomain and data-parallel lower-upper relaxation sweep at the subdomain boundary. A detailed description of DP-SGS was included in [14,15].

For turbulence consideration, a modified shear-stress transport (SST) [15] turbulence model from Menter's SST [16] model is used to improve the predictability in the massively separated flowfields.

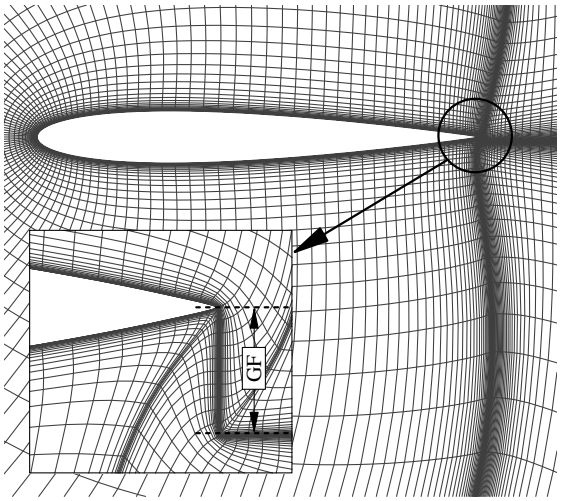

Fig. 1 Grid topology for Gurney flap (GF) airfoil.

The model was modified from the basic premise that shear-stress tensor of eddy viscosity is proportional to strain tensor rather than vorticity. A more detailed description of numerical methods can be found in [15].

For steady calculations, maximum subiteration and subiteration convergence criteria were set to 100,000 and −6 respectively. If a solution has oscillatory characteristics by exceeding static stall angle, unsteady calculation is performed and time-averaged aerodynamic force values are obtained. For dynamic stall calculations, a single period is divided by 1400 physical time steps, and the number of maximum subiteration and residual were set to 200 and −6, respectively. Usually, 50 subiterations were enough for convergence. A 259×61 C-type grid with 159 points on the airfoil surface was used for baseline clean airfoil and a 279×61 C-type grid was used for the 1.0% Gurney flap case. The Gurney flap was treated as a wall line with 20 grid points. If its length is increased by twice (2% C Gurney flap), grid points on the Gurney flap are increased linearly (40 points).

Minimum normal grid spacing was reduced to 1×10^{-5} chords, ensuring a value of $y^+ < 1$ everywhere on the airfoil surface. Figure 1 shows the computational grids of the NACA 0012 with 1% of Gurney flap.

Temporal and spatial convergence tests and selection of appropriate turbulence modeling were performed for an oscillating NACA 0012 airfoil and comparison is made with experimental data. Pitch angle varies as $\alpha(t) = 15 + 10 \deg \sin(\omega t)$, where the reduced frequency is 0.151, the freestream Mach number is 0.283, and Reynolds number is set as 3.45×10^6 as in the experiment in [17]. A C-type 127×45, 259×61, and 323×91 grid is used for spatial convergence check, and physical time step (dt) is varied with 0.1022, 0.0510 (single period divided by 1440 physical time steps), and 0.0255 is used for temporal accuracy check.

Figure 2 shows the variation of aerodynamic coefficients during the last period of a total of three periods. It is seen from the figure that there is no significant difference between the SST and the present modified SST model during pitch-up motion. The angular location of stall and maximum lift coefficients are almost the same among the three turbulence models. However, the BSL model (baseline model, standard k–ϵ model, and Wilcox k–ω model are mixed with a blending function by Menter [16]) has a large discrepancy with experiments in the return to unstalled region. And, the SST model has great fluctuation of lift, drag, and moment coefficients at just after the region of pitch-down motion and the reattachment region. Unlike the preceding two models, the modified SST model has better agreement with experimental data. Therefore, all calculations were performed with the modified SST turbulence model.

With the spatial grid fixed to 259×61, temporal convergence was investigated by varying physical time step. There is no significant difference of aerodynamic coefficient by changing physical time step

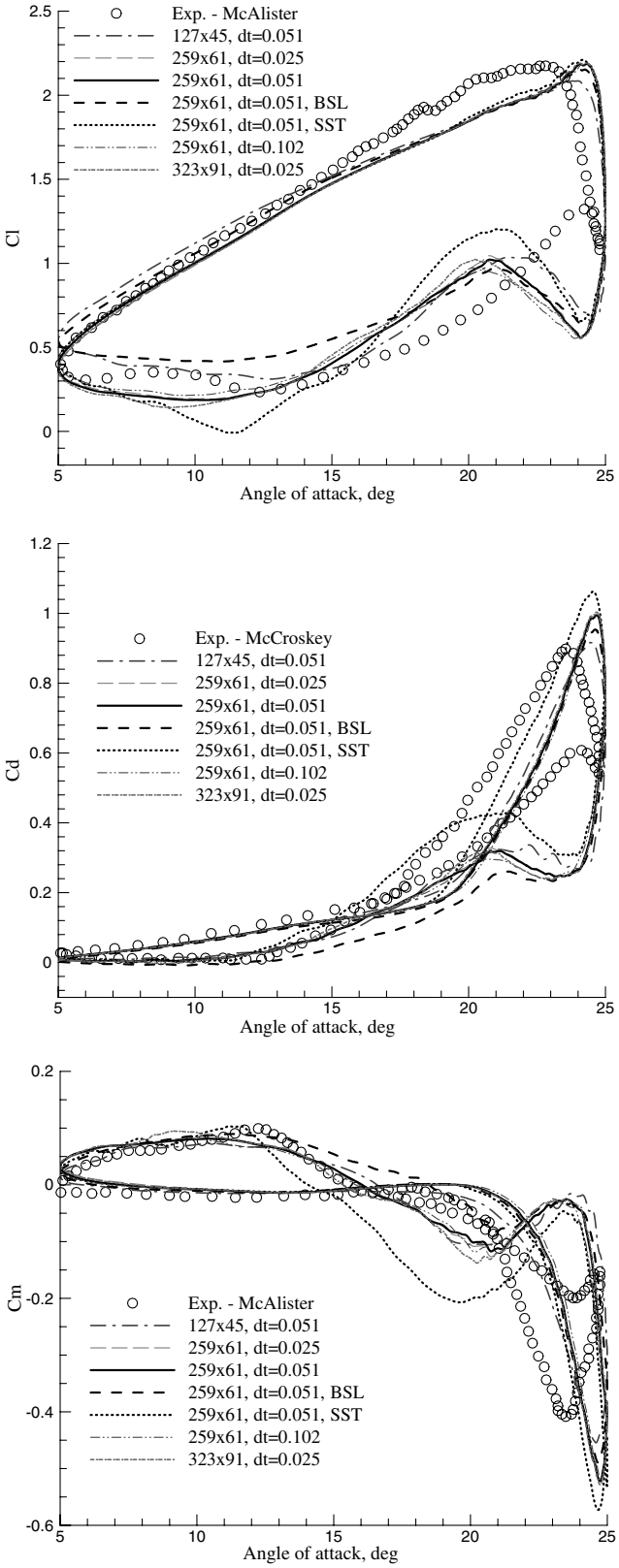

Fig. 2 Hysteresis effects for deep stall obtained with three models: NACA 0012, $M_\infty = 0.283$, $Re = 3.45 \times 10^6$, $\alpha(t) = 15 + 10 \deg \sin(\omega t)$, $k = 0.151$.

with the 259×61 size grid. However, in the case of reduced grid size to 127×45 with same time step, the lift hysteresis has a large discrepancy in the unstalled region as in the BSL model, and the drag and moment coefficients have some oscillation just after pitch-down motion. A 323×91 grid, which has 1.5 times larger grid points than the baseline grid, did not show significant improvement.

So, we chose a 259×61 C-type grid with 0.0510 physical time steps for efficient calculation. All calculations were run on the HAMEL cluster at Korea Institute of Science and Technology Information, which has a total of 512 CPUs composed with Zeon 2.4 GHz CPU and 1.5 GB memory. In airfoil table generation, about 400 cases are calculated and a total of 60 h are required with 8 CPUs. In a dynamic stall case, about $3 \sim 4$ h are required for each case with the same hardware.

Research Approach

Static Calculation

A series of numerical calculations were performed to investigate the steady aerodynamic characteristics of the Gurney flap for various Mach numbers and angles of attack. The ranges of Mach number (0.3–1.0) and angles of attack (−20–20 deg) were set to include the stall and transonic regions of interest.

Compared with the clean NACA 0012 airfoil, the calculations were performed under 0.5, 1, 2, and 4% height Gurney flaps, respectively. To isolate the effect of the Gurney flap, the airfoils with different camber or thickness were not included in the calculation. The NACA 0012 airfoil was chosen for the baseline airfoil because there were plenty of experimental data whose reliability was critically assessed by McCroskey [18]. Therefore, it was believed that the NACA 0012 was particularly suitable for the validation of the numerical results. More than 40 wind tunnel tests for the NACA 0012 were systematically evaluated by McCroskey to categorize the experimental results into four groups according to their reliability [18]. The statistical correlations were obtained for group 1, which is the most reliable data set to yield the baseline database for the validation of experiments and numerical simulations. Bousman used the similar procedure developed by McCroskey to filter the performance characteristics of SC1095 and SC1095R8 airfoils [19].

The validations of the numerical results were made for the data correlations of McCroskey [18] and C81 format data of the NACA 0012 in CAMRAD II, if necessary. The calculations were performed for fully turbulent flows with the Reynolds number of 6.544×10^6 based on the freestream Mach number $M = 1$. The Reynolds number at an arbitrary Mach number is then calculated as in Eq. (2). This relation is usually an approximation of the true relation between Reynolds number and Mach number for the airfoil data. Next, the aerodynamic performance of the Gurney flap was scrutinized for the rotor operating conditions to evaluate the viability for rotorcraft application.

$$Re = Re_{\text{ref}} \times M_\infty / (M_{\text{ref}} = 1) \quad \text{where } Re_{\text{ref}} = 6.544 \times 10^6 \quad (2)$$

Dynamic Calculation

The numerical experiments were performed with respect to reduced frequency and amplitude to examine the unsteady aerodynamic features of the Gurney flap. The unsteady airfoil motion was defined as

$$\alpha(t) = \alpha_0 + \alpha_1 \sin(\omega t) \quad (3)$$

The calculations were validated for the wind tunnel tests at the NASA Ames Research Center in the late 1970s and early 1980s. McAlister et al. [17] tested eight different airfoils in NASA Ames' 7×10 ft wind tunnel. Each airfoil was tested on the same test rig. Test data were obtained for mean angles of 10 and 15 deg and alternating angles of 5 and 10 deg. The reduced frequency was varied from 0.02 to 0.2 with 0.02 increments and the Reynolds number was fixed at 4 million for a Mach number of 0.3. For each airfoil, a total of 90 numerical experiments were performed with the variation of mean angles of attack, alternating angles of attack, and reduced frequency. Table 1 shows the 40 numerical experimental points. An additional 50 numerical experiments are randomly distributed within lower and upper boundaries of each variable in Table 1. The calculations were continued until the aerodynamic coefficients attained full periodicity (usually 3 periods).

Table 1 Dynamic stall calculation parameter

	Minimum	Maximum	Increment
Mean angle	10	15	5
Alternating angle	5	10	5
Reduced k	0.02	0.2	0.02

Bousman [20] suggested the dynamic stall function to compare the relative aerodynamic performance of different airfoils and applied the function to analyze the tests of McAlister et al. [17], systemically. The dynamic stall function can be quantified by fitting a second order polynomial to the data and it shows the correlations between the extrema of the aerodynamic coefficients. In general, the extrema of the aerodynamic coefficients such as the maximum lift, the maximum drag, and the minimum pitching moment are not coincident in time. However, they are related to the movement of the dynamic stall vortex over the airfoil and they can be used to quantify the aerodynamic features of the dynamic stall.

In the present study, the comparison of the dynamic stall functions was first made between the calculations and McAlister's tests for the NACA 0012 airfoil [17]. Then, the dynamic stall functions were successively derived for 0.5, 1, 2, and 4% height Gurney flap to analyze the quantitative as well as qualitative differences from the baseline airfoil.

Results and Discussion

Static Aerodynamic Characteristics

The helicopter operating modes can be categorized into hovering, transient flight, and forward flight. For each flight mode, the relation between the lift and Mach number of the rotor airfoil is shown in Fig. 3.

The primary aerodynamic requirements of a rotor airfoil can be summarized as follows:

1) For the advancing side in forward flight: supercritical performance at low lift level, with near zero pitching moment.

2) For the retreating side in forward flight: high lift at Mach 0.3–0.5 to avoid excessive control load and aeroelastic instability due to dynamic stall, with near zero pitching moment.

3) For hovering: low drag or lift-to-drag ratio at around $Cl = 0.6$ and $M_\infty = 0.6$.

Therefore, to evaluate the viability and potential of the Gurney flap as a rotor airfoil, it should be assessed based on the preceding aerodynamic requirements. In this sense, it is useful to examine the

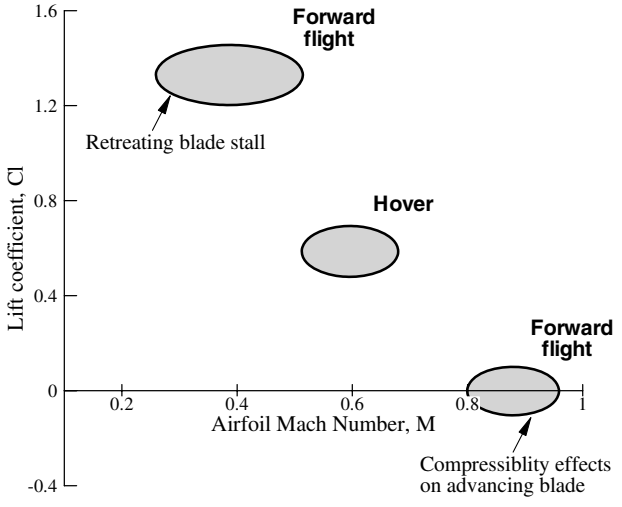

Fig. 3 Typical rotorcraft flight regime.

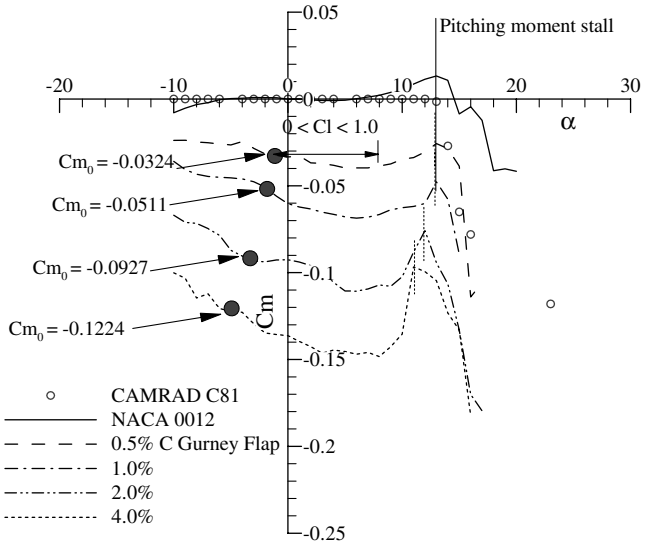

Fig. 4 Pitching moment for various Gurney flap heights at $M_\infty = 0.3$.

calculation results based on the airfoil design criteria suggested by Dadone [21].

Retreating Side in Forward Flight: Cm_0 at $M_\infty = 0.3$

It is necessary to reduce the excessive nose-down pitching moment which occurs due to the dynamic stall in high forward flight. Because rotor blades are usually quite supple in torsion, a high amplitude torsional motion can persist as the blade continues to rotate. This phenomenon, called stall flutter, results in high structural loads and high power requirements.

Figure 4 shows the pitching moments for various Gurney flap heights and the calculation results are compared with C81 data in CAMRAD II. As suggested by other researchers, the Gurney flap tends to increase effective camber and the pitching moments monotonically decrease with the Gurney flap height accordingly.

The calculated pitching moment of the NACA 0012 airfoil has a good agreement with the C81 data and it generally predicts the moment stall angle with good accuracy. For small Gurney flap heights less than 2% C, the pitching moment of the Gurney flap remains almost constant in the prestall region of $0.0 < Cl < 1.0$, which is considered an important factor in determining the rotor aeroelastic stability and control load. However, it can be found that the pitching moment has negative gradient even in the prestall region with the increase of the Gurney flap height, as can be seen in Fig. 4.

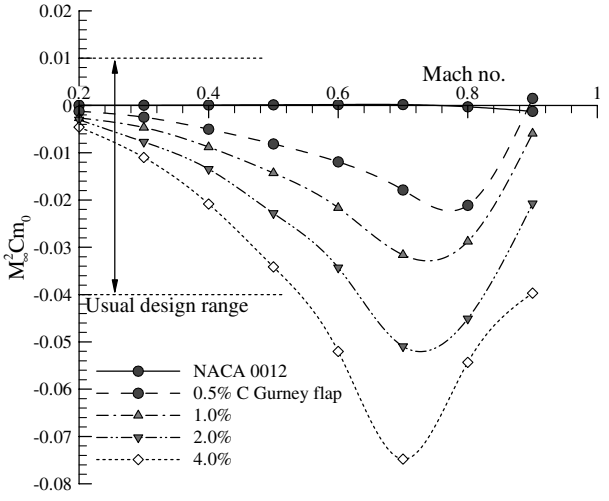

Fig. 5 Zero-lift pitching moment with compressibility effects.

Because the dynamic stall usually occurs at low Mach number, the relative features of different airfoils were compared in terms of Cm_0 at $M_\infty = 0.3$. It is shown that Cm_0 decreases monotonically with the Gurney flap heights. Considering that the general design criteria for the pitching moment is about -0.02 which is suggested by Dadone [21], Cm_0 of -0.03242 for the 0.5% Gurney flap seems to be relatively large. For the 4% height Gurney flap, Cm_0 reaches even -0.12238, which is almost four times greater than that of the 0.5% Gurney flap. In this sense, the 0.5% Gurney flap seems to be close to the limit in terms of pitching moment design criteria.

However, the modern rotor airfoil design tends to allow higher Cm_0 airfoil as in BERP and UH60 because the high pitching moment at the main lifting section can be alleviated by using the reflex airfoil at the inboard region, thereby reducing the overall torsional moment of the rotor blade [22]. For example, RAE 9645 airfoil implemented at the main lifting section of BERP has the pitching moment of about -0.0305.

Although the Cm_0 is commonly used for the design criteria to compare the overall pitching moment characteristics of different airfoils, it does not represent the actual magnitudes of the pitching moment in that the dynamic pressure is not considered. Hence, the pitching moment multiplied by dynamic pressure is more appropriate for relative comparison of the airfoils. To partially account for this effect, $M_\infty^2 Cm_0$ with various Mach numbers are depicted for each airfoil in Fig. 5. The design range in the figure was suggested by Dadone who surveyed the currently used rotor airfoils [21].

As it can be found in the figure, in contrast to the NACA 0012 for which pitching moment is nearly zero even in the transonic region, the Gurney flap airfoils have minimum values around the Mach tuck. It is obviously shown that the moment stall is promoted with the increase of the Gurney flap height.

It is interesting to note that the usual design range is not violated until the Gurney flap heights exceed 2%. In conclusion, although the nose-down pitching moment increases monotonically with the flap height, the Gurney flap can be used as a rotor airfoil as long as the flap height is within the appropriate range (less than 2% in the present study).

Retreating Side in Forward Flight: $Cl_{\max}$ at $M_\infty = 0.4$ and 0.5

As the forward flight speed increases, the aerodynamic loading becomes more concentrated on the blade tip region. Accordingly, the blade tip region is more vulnerable to the stall than the inboard region. Hence, to increase the stall limit, the $Cl_{\max}$ of the rotor airfoil should be large enough at the Mach number 0.3–0.5. On the contrary, the reverse flow due to stall has little effect on the rotor thrust and torsional moment because the dynamic pressure is small at the

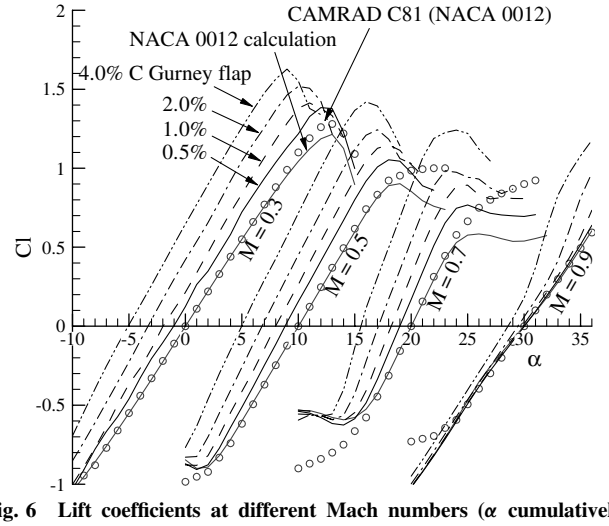

Fig. 6 Lift coefficients at different Mach numbers (α cumulatively shifted with Mach number increases, 5 deg /0.1 Mach).

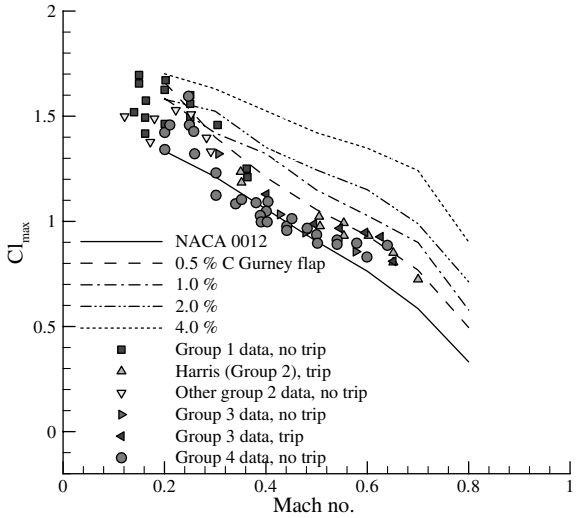

Fig. 7 Maximum lift coefficients with Mach number for various Gurney flap heights.

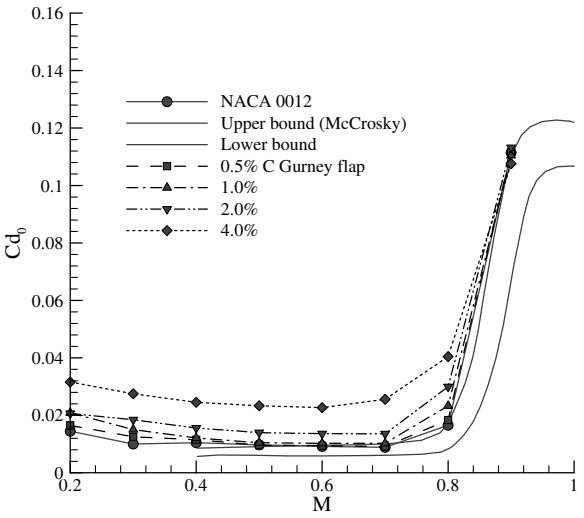

Fig. 8 Comparison of zero-lift drag coefficients with Mach number.

inboard region. Hence, the $Cl_{\max}$ at $M_\infty = 0.4$ and 0.5 represents the requirements for the rotor airfoil at the blade outboard region.

For a given lift, the separation condition is known to be a function of freestream Mach number and the shape of the airfoil. In general, local supersonic region begins to build when the freestream Mach number reaches around 0.5 and it is preferable that the stall have gradual and smooth features as in the trailing-edge stall to suppress an abrupt control load variation.

Figure 6 shows the comparison of lift coefficients of each airfoil with different Gurney flap heights at various Mach numbers.

As is known, the maximum lift coefficient monotonically increases with the Gurney flap height. It is confirmed in the present study that the lift-enhancement capability of the Gurney flap is maintained irrespective of freestream Mach number. The airfoil with 0.5% Gurney flap has about 16% greater maximum lift coefficient than the baseline clean airfoil. One may observe that the stall is slightly promoted due to the Gurney flap. For example, it is about 3 deg earlier that the stall occurs for 4% Gurney flap. However, based on the stall angle minus zero-lift angle ($\alpha_{\text{stall}} - \alpha_0$), which is physically more important, the difference is negligible.

Compared with C81 data, the lift coefficient of the baseline airfoil is shown to be in a good agreement with the calculations. The $Cl_{\max}$ and stall angle are predicted with good accuracy but there is some discrepancy found in the poststall behaviors in the lift coefficient curve at the transonic region.

The $Cl_{\max}$ with respect to the Mach number are compared with that of McCroskey [18] in Fig. 7. It is clearly shown that the inclusion of the Gurney flap can greatly increase the $Cl_{\max}$. The NACA 0012 calculations are mostly in agreement with group 4 and there is some discrepancy with group 1 data which was considered most reliable. It is thought that this discrepancy partially stems from different flow conditions and the existence of trip. Even with some discrepancy with group 1 data, the numerical data are shown to lie within the boundary of experimental data.

It is shown that the $Cl_{\max}$ increases with the Gurney flap height and the airfoil with 4% Gurney flap has almost 37% greater $Cl_{\max}$ than the baseline airfoil at $M_\infty = 0.2$. It is again confirmed here that the Gurney flap is an efficient device to enhance the lift even at the transonic region.

Advancing Side in Forward Flight: Drag Divergence Mach Number

The zero-lift drag divergence Mach number represents the aerodynamic characteristics of the rotor airfoil at the outboard region of the blade in forward flight. Although M_{DD} is not the best index to quantify the abrupt drag rise due to the compressibility effects, it is widely used due to its simplicity and reliability.

To clarify the drag characteristics of each airfoil at the transonic region, zero-lift drag coefficient for various airfoils are shown in Fig. 8. The solid lines in the figure represent the lower and upper limits of the wind tunnel test of group 1 in McCroskey [18]. The drag divergence Mach number was defined as the Mach number at which the slope of Cd_0 curve reaches 0.01 or the change in drag is 0.002 (20 counts) above its incompressible value. The present paper chose the latter definition. As there were not enough data points near a transonic region, a quadratic spline curve of Cd_0 was used to determine M_{DD}. Table 2 shows some main discussed parameters in this paper including M_{DD}. As shown in Fig. 8, Cd_0 of the NACA 0012 airfoil is generally on the border of the upper limit, which is considered one of the evidences regarding the reliability of the present calculation results.

No significant difference in M_{DD} with Gurney flap height is observed. It is rather surprising because this means that the Gurney

Table 2 Theoretical prediction for five rotor airfoils

	Requirements	0.0% *C* GF	0.5% *C* GF	1.0% *C* GF	2.0% *C* GF	4.0% *C* GF
1	Cm_0 at $M_\infty = 0.3$	0.00000	−0.03242	−0.05113	−0.09265	−0.12238
	$Cl_{\max}$ at $M_\infty = 0.4$	1.05828	1.21043	1.32191	1.35168	1.52555
	M_{DD}	0.7532	0.7586	0.7509	0.7512	0.7343
2	Cd for $M_\infty = 0.6$ and $Cl = 0.6$	0.01367	0.01194	0.01265	0.01542	0.02462
	$Cl_{\max}$ at $M_\infty = 0.5$	0.90490	1.05525	1.14901	1.24435	1.42150
	Cd_0 at $M_\infty = M_{\text{DD}} + 0.02$	0.01339	0.01513	0.01764	0.02324	0.03159
3	M^2Cm_0 at M_{DD}	0.00003	−0.02061	−0.03331	−0.05295	−0.06867
	Type of stall	LE stall	LE stall	LE stall	LE stall	LE stall
	Cd_0 at $M_{\text{DD}} - 0.1$	0.00886	0.00900	0.00949	0.01371	0.02318

[a]LE stall: leading edge stall.

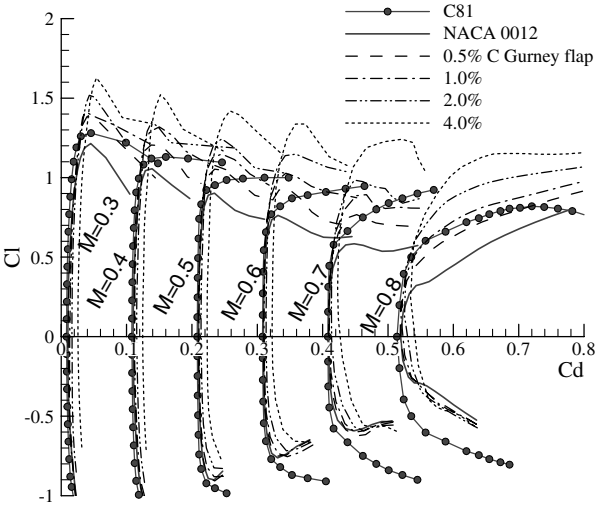

Fig. 9 Drag polars of Gurney flap airfoils at different Mach numbers (*Cd* cumulatively shifted with Mach number increases, 0.1 *Cd*/0.1 Mach).

flap has little adverse effects on the M_{DD} at the transonic region in spite of the increase of Cd_0 for 4% Gurney flap. It is also worthwhile to note here that unless the Gurney flap height exceeds 2% *C*, the increase in Cd_0 is negligible for all Mach numbers.

When the freestream velocity exceeds the M_{DD}, the wave drag due to the shock wave rapidly rises. Hence, it is advantageous to keep the slope of drag rise after M_{DD} because the advancing blade of the rotor usually operates at the Mach number greater than M_{DD}. As is shown in Fig. 8, there is no meaningful difference in the slope of drag rise for each airfoil.

In conclusion, the Gurney flap with less than critical height (presently 2%) does not have significant drag penalty regardless of Mach number. This conclusion should be rigorously verified by experimental data.

Hovering: Drag Coefficient at $M_\infty = 0.6$, $Cl = 0.6$

This criterion is used to represent the aerodynamic performance of an airfoil in hovering. Because the drag coefficient at the prestall region largely results from the profile drag due to friction, it is desirable to keep the laminar flow over the upper surface as long as possible to reduce the overall drag coefficient. However, the transition from laminar to turbulent flow is not included because the present calculations assume the fully turbulent flows.

Figure 9 depicts the drag polars for various Gurney flap heights from 0.0 to 4% *C* with Mach numbers. The figure exhibits that there exists little penalty in zero-lift drag as long as the Gurney flap height is less than 0.5%, but in the case that the Gurney flap height is greater than 2%, significant drag penalty occurs, which qualitatively agrees with the experimental evidence by Myose et al. [6]. To examine more closely, the drag polars at $M_\infty = 0.3$ and 0.6 are magnified in Fig. 10. From the comparison with C81 data of CAMRAD II, it is seen that the calculation of the baseline airfoils predicts a little higher drag coefficient. However, because the overall predictions are reasonable, it can be implied that the qualitative comparisons could be made for different Gurney flap heights.

It is interesting to note that there is a critical value of lift at which the drag of the Gurney flap airfoil becomes less than the baseline airfoil. Moreover, this critical value has a tendency to decrease with the Mach number. For example, at $M_\infty = 0.3$, the critical value of lift is about 0.87 but 0.12 at $M_\infty = 0.6$. It is also observed that the critical value has a tendency to increase with Gurney flap height.

This is of importance in that for the typical hovering condition, the Gurney flap airfoil might generate less drag unless the flap heights exceed 2% *C*. By reducing the sectional drag coefficient, the required power to hover can be reduced. Therefore, the proper use of the Gurney flap can improve hovering performance extensively.

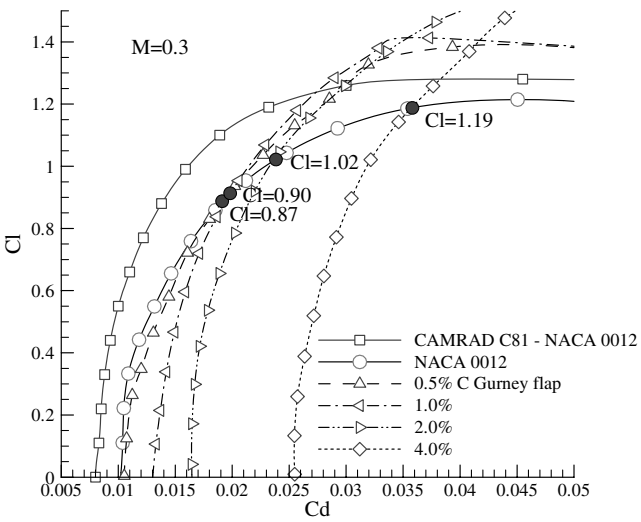

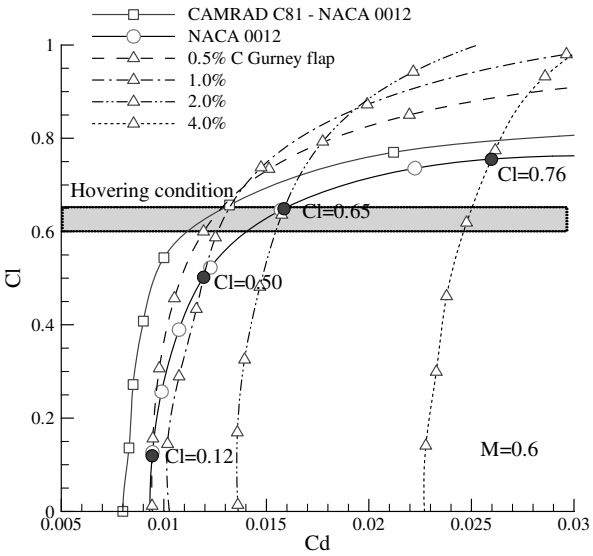

Fig. 10 Magnified drag polars at $M_\infty = 0.3$ and 0.6.

Thus, the airfoil with the Gurney flap of which the size is shorter than 2% *C* has smaller *Cd* than that of the baseline airfoil for the hovering conditions as $M_\infty = 0.6$ and $Cl = 0.6$.

Comparing the drag coefficients of each airfoil at $M_\infty = 0.4$ and 0.7 in Fig. 11, it can be observed that the Gurney flap airfoil has a generally higher drag coefficient. Because of the increased effective camber, the drag is no longer symmetric with respect to the vertical axis, which implies that the Gurney flap has minor impact on the drag in the negative angle of attack. In other words, its effect on the drag is diminishing when angle of attack goes negative, because the Gurney flap is immersed in the wake region of the airfoil. Figure 12 shows pressure contours around the NACA 0012 airfoil with 4% chord Gurney flap. In positive angle of attack, the Gurney flap is exposed to flow directly, whereas in negative angle of attack it is under the influence of the airfoil wake. As a result, additional pressure rise is found in positive angle of attack when the Gurney flap is attached.

As is expected, the drag penalty increases with the Gurney flap heights. However, the lift increase is much greater than the drag penalty, the drag of the Gurney flap airfoil is smaller for a given lift coefficient, which is true irrespective of Gurney flap heights.

As Bousman described in [23], when designing a rotor airfoil to increase Cl_{max}, the lift-to-drag ratio should be verified. Otherwise, the overall aerodynamic performance deteriorates. Hence, the rotor airfoil should be designed to increase the lift-to-drag ratio under normal operating conditions of the rotor blade. Figure 13 shows that

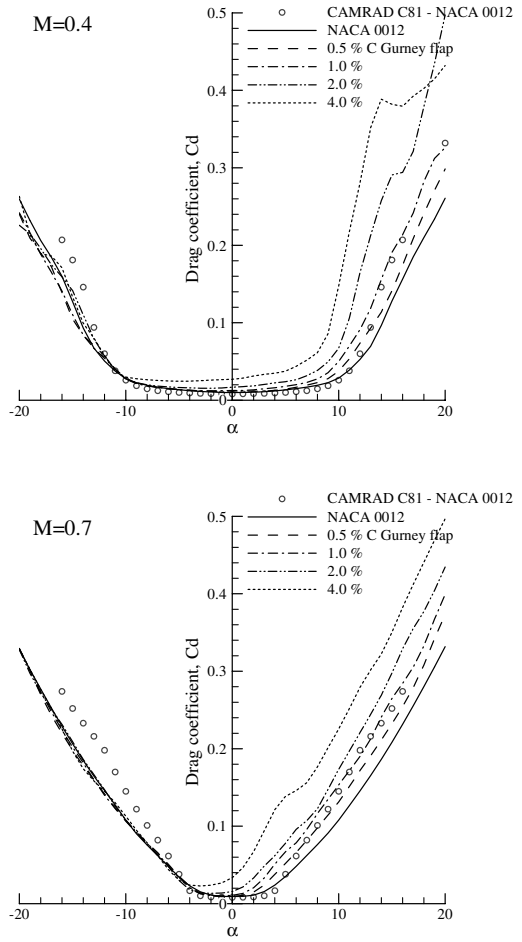

Fig. 11 Comparison of drag coefficients at $M_\infty = 0.4$ and 0.7.

the Gurney flap airfoil has a characteristic which conforms to this criterion. It should be noted that the calculated lift-to-drag ratios are underpredicted by more than 50% in comparison with those in McCroskey [18], which is the common limit of the modern CFD codes as shown by Smith et al. [24]. The Gurney flap airfoil has greater lift-to-drag ratios for all Mach numbers as long as the flap height is less than 2% *C*. As mentioned earlier, this improvement is attributed to the rapid increase of lift, not to the reduction of drag. On the other hand, the improvement in the lift-to-drag ratio vanishes when the Gurney flap height exceeds 2% *C*, which is obviously due to the considerable increase of drag.

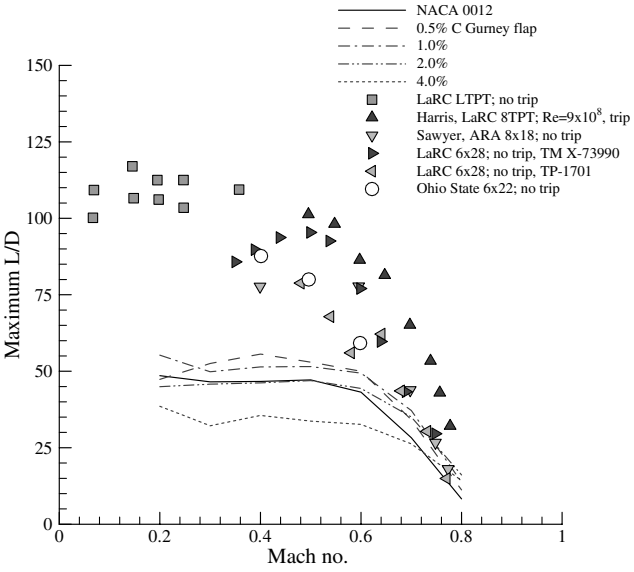

Fig. 13 Comparison of maximum lift-to-drag ratio with Mach number.

Conclusively, it is confirmed that there is a critical Gurney flap height for which the Gurney flap airfoil has superior characteristics in hovering condition (presently less than 2% *C*).

In Figs. 14 and 15, the Cl_{max} is compared with respect to M_{DD} at $M_\infty = 0.4$ and 0.5, respectively. The figure summarizes the overall aerodynamic characteristics. The solid line in the figure is the known performance boundary of the existing rotor airfoils surveyed by Dadone [21]. It exhibits the drastic increase of Cl_{max} with the Gurney flap height, with only a little decrease in M_{DD}. Hence, the Gurney flap may be regarded as a viable device to improve the aerodynamic characteristics at the retreating side of the helicopter rotor with the compressibility drag rise kept minimum at the advancing side. As is well known, the Gurney flap may increase the nose-down pitching moment but it does not exceed the allowable design range when the flap height is less than 2%.

Unsteady Aerodynamic Characteristics

To improve the maneuverability and extend the flight envelope of the helicopter, it is the maximum thrust that should be increased.

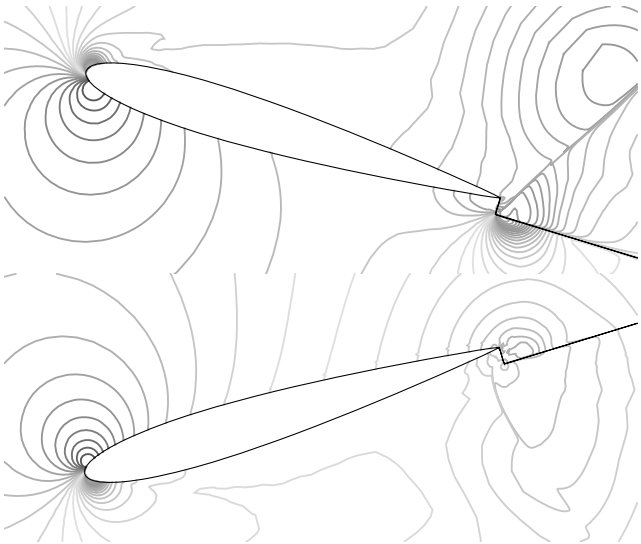

Fig. 12 Pressure distribution of NACA 0012 airfoil with 4% *C*Gurney flap at +17 and −17 deg angle of attack.

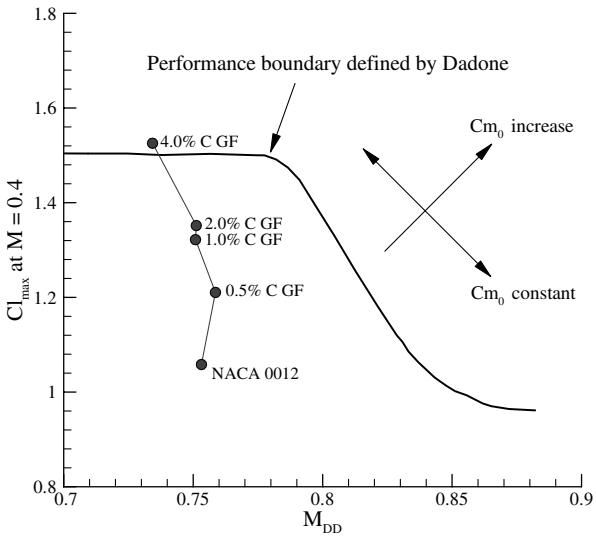

Fig. 14 Trends of maximum lift and drag divergence Mach number with Gurney flap height at $M_\infty = 0.4$.

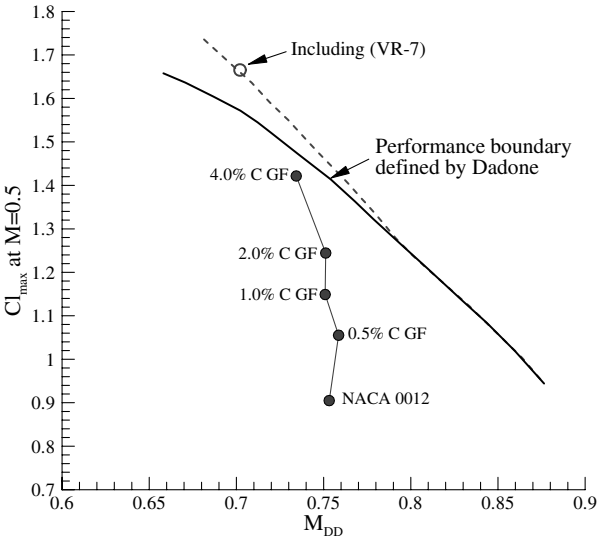

Fig. 15 Trends of maximum lift and drag divergence Mach number with Gurney flap height at $M_\infty = 0.5$.

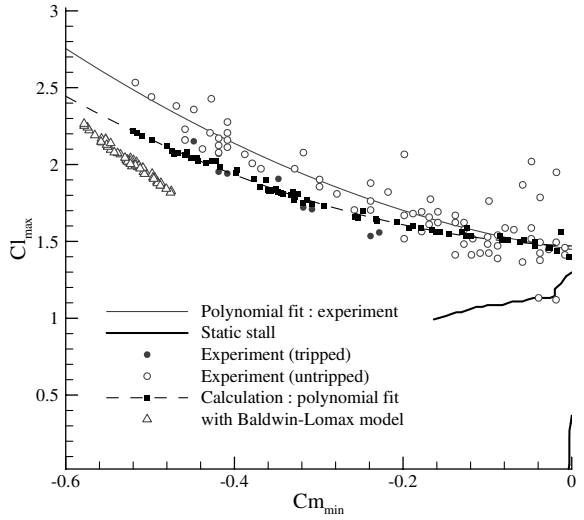

Fig. 16 $Cl_{\max}$ as function of $Cm_{\min}$ with comparison between dynamic stall test and calculation for NACA 0012 airfoil.

Thus, the suppression of dynamic stall vortex and the minimization of its strength for a given flight condition does not necessarily imply a performance improvement because it only shifts the flow conditions at which the dynamic stall occurs. Consequently, to evaluate the relative performance of the airfoils, the pitching moment and drag should be compared at the same lift condition. The simple comparison of aerodynamic performance for given mean angle of attack (α_0), alternating angle of attack (α_1), and reduced frequency is not appropriate.

During the dynamic stall, the lift, pitching moment, and drag undergo drastic changes as the leading-edge vortex moves along with the upper surface of the airfoil. In general, the extrema of the aerodynamic coefficients such as the maximum lift, the maximum drag, and the minimum pitching moment are not coincident in time. However, they are related with the movement of the dynamic stall vortex over the airfoil and can be used to quantify the aerodynamic features of the dynamic stall. Bousman suggested the second order polynomial correlation called "dynamic stall function" between the extrema of the aerodynamic coefficients during the dynamic stall, which is defined as [20]

$$\begin{aligned} Cl_{\max} &= a_0 + a_1 Cm_{\min} + a_2 Cm_{\min}^2 \\ Cl_{\max} &= b_0 + b_1 Cd_{\max} + b_2 Cd_{\max}^2 \end{aligned} \tag{4}$$

The dynamic stall function is useful to comparatively assess the aerodynamic performance of the airfoil. From the detailed analyses of the experiments, the dynamic stall functions are almost constant over the Reynolds range from 0.1 to 4 million [20]. Such constant result of dynamic stall function makes sense because the dynamic stall is a phenomenon dominated by the leading-edge vortex. Hence, considering the computation time, this study does not include the effects according to the Reynolds number.

Even with the remarkable advances of computational fluid dynamics for the decades, there still exists a significant uncertainty for the unsteady problems such as the dynamic stall. Although there is a slight variation depending on the turbulence model, the modern numerical codes still can not predict with sufficient accuracy the nose-down pitching moment and drag for the deep stall problems with massive separation. However, it is assumed in the present study that by means of systematic numerical computations, despite its limitations, the qualitative comparisons can be made between the airfoils except at the deep stall region.

Code Validations

For code validation, the comparison was made for the computational results of the NACA 0012 airfoil with the experimental data of McAlister et al. [17], later summarized by Bousman [20]. The correlation between the $Cl_{\max}$ and $Cm_{\min}$ is exhibited in Fig. 16. The numerical results are generally in good agreement with the experiments at the light stall region. However, for the deep stall region, in the left part of the figure, the calculation tends to underpredict the pitching moments. Even currently, there is no CFD code that can exactly capture the dynamic stall phenomena. It should be noted here that the numerical results fit better with the tripped data which is similar to the present assumption of fully turbulent flows. However, no meaningful comparisons could be made because of an insufficient amount of experimental data. To account for the influence of the turbulence model, the results from the Baldwin–Lomax model were also shown in the figure. It is clearly shown that the Baldwin-–Lomax model does not yield reliable results for the $Cl_{\max} - Cm_{\min}$ correlation.

Figure 17 shows the correlation between $Cl_{\max}$ and $Cd_{\max}$ of the NACA 0012 airfoil. There is a remarkable agreement between the numerical results and experimental data. The $Cl_{\max}$ has nearly linear relation with $Cd_{\max}$ and the data scattering is very small. In the $Cl_{\max} - Cd_{\max}$ correlation, the Baldwin–Lomax model shows

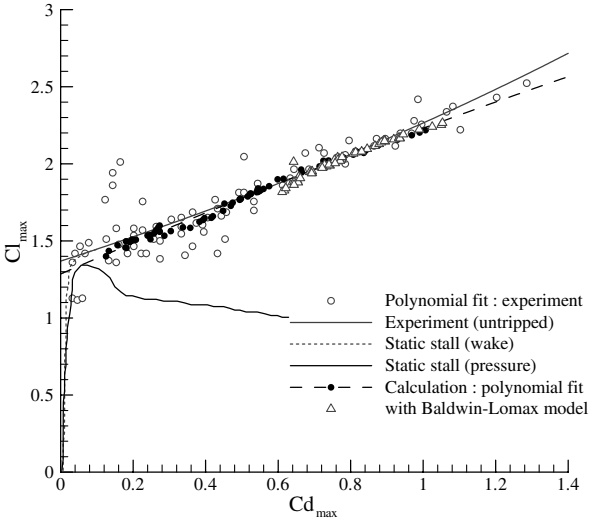

Fig. 17 $Cl_{\max}$ as function of $Cd_{\max}$ with comparison between dynamic stall test and calculation for NACA 0012 airfoil.

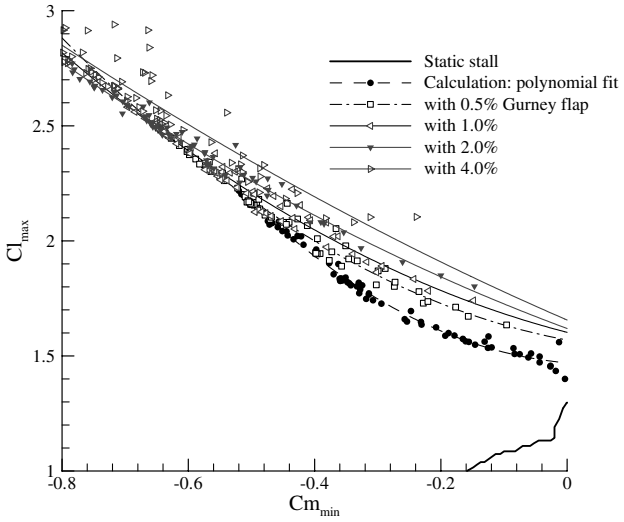

Fig. 18 $Cl_{\max}$ as function of $Cm_{\min}$ with different Gurney flap heights.

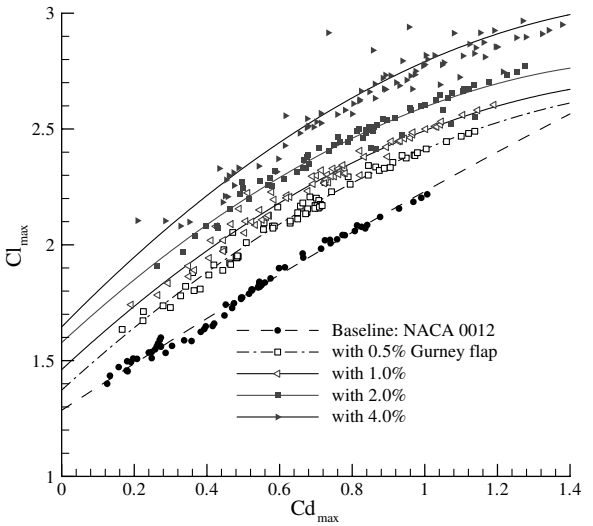

Fig. 20 $Cl_{\max}$ as a function of $Cd_{\max}$ with different Gurney flap heights.

similar trends with the experimental data as well as with the results from the SST model. Although there exist slight differences in the coefficients of dynamic stall functions depending on the turbulence model, the general trends are well predicted by the numerical calculations. Hence, it can be concluded that the qualitative comparison between the different airfoils is possible by means of present numerical approaches though it needs further studies to confirm its validity.

Comparison of Unsteady Aerodynamic Performances Between the Airfoils

The dynamic stall functions of the Gurney flap airfoils with different heights from 0.5 to 4% C are shown in comparison with that of the NACA 0012 airfoil in Fig. 18. By looking at the correlation between $Cl_{\max}$ and $Cm_{\min}$ first, it is obvious that the greater the Gurney flap height is, the better the aerodynamic performance improves. As mentioned earlier, because the aerodynamic performance between the different airfoils should be compared for the same lift condition, the higher location of the line in the figure means the better performance. As it can be found in Fig. 18, the Gurney flap airfoils have superior characteristics to the baseline NACA 0012 airfoil for most dynamic stall ranges. In other words, the airfoils with the Gurney flap have the smaller pitching moment than the baseline airfoil for a given lift. However, the performance increment seems to decrease with the Gurney flap height as shown in Fig. 19. In the figure, δa_0 and δb_0 is the difference of intercepts of dynamic stall function between the Gurney flap applied cases and the baseline, and the values are related to the relative location of the $Cl_{\max}$ line compared with baseline.

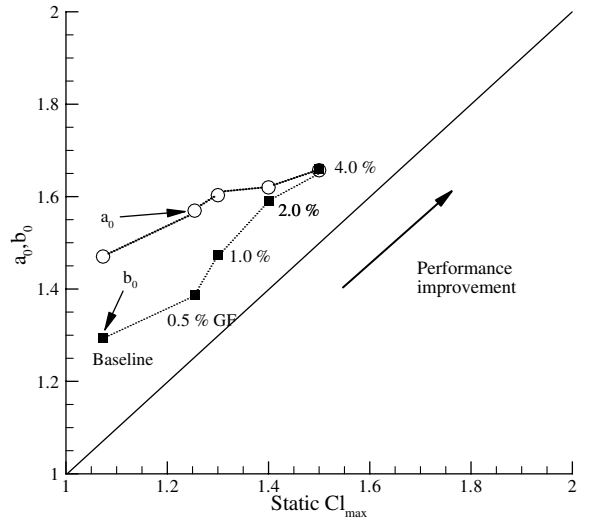

Fig. 21 Trends of dynamic stall function intercepts with Gurney flap height.

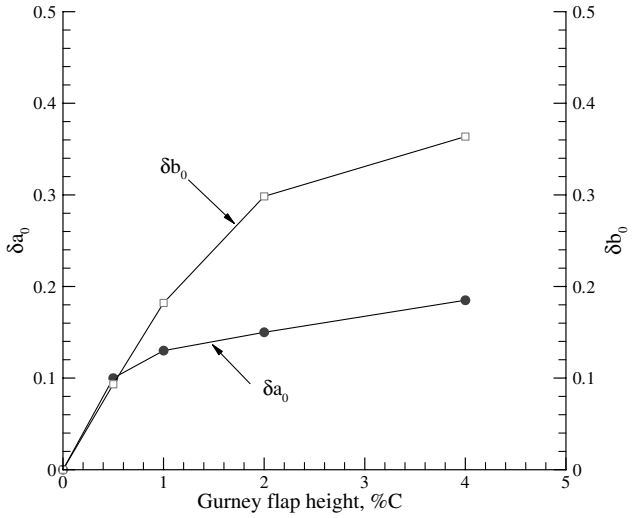

Fig. 19 Increments of dynamic stall function coefficient with Gurney flap heights.

Considering the static aerodynamic results, it is rather surprising that there is no pitching moment penalty due to the Gurney flap during the unsteady motion. It is indicated that the lift-enhancement far outweighs the pitching moment penalty. Moreover, it should be noted that no substantial differences can be found in the deep stall region. It requires further study to clarify the reason because it is ambiguous at present whether this is due to the limitation of the numerical codes or due to the actual physics.

It is also found from the $Cd_{\max} - Cl_{\max}$ dynamic stall functions of Fig. 20 that the airfoil with the Gurney flap has superior performance to the baseline airfoil. That is, for a given drag, the Gurney flap airfoil has higher lift and the lift increment increases with the flap height. However, it is found that the lift increment is nonlinear with the flap height. One thing to note is that the data scattering (the variation) increases with the flap height, especially for the 4% height Gurney flap.

As shown in the Fig. 19, the dynamic stall functions of each airfoil have similar profiles despite the difference in the magnitude depending on the Gurney flap height. As the dynamic stall functions approach zero drag and zero pitching moment, the intercepts, a_0 and

b_0 become close to the static maximum lift coefficient. In Fig. 21, the intercepts, a_0 and b_0 are shown as a function of static $Cl_{\max}$, which is suggested by Bousman [20]. The intercepts, a_0 and b_0 show a lift increment over the static $Cl_{\max}$ of 0.13–0.21. The intercept values are largely defined by the measurements for light stall conditions where no dynamic stall vortex is shed. In this sense, the intercepts indicate the incremental lift in unsteady motion without a moment or drag penalty. That is, the greater value of a_0 and b_0 means the higher lift increment in the unsteady motion. Therefore, the airfoils fitted with the Gurney flap have better performance than the NACA 0012 and the magnitude of improvement consistently increases with the Gurney flap height.

In summary, the Gurney flap has improved the lift performance in light to moderate dynamic stall conditions but the magnitude of improvement decreases with the flap height. Hence, it can be concluded that the Gurney flap has advantages for all flap heights considered in the present study in terms of unsteady aerodynamic performance.

Conclusions

In the present study, the aerodynamic characteristics of the Gurney flap were comprehensively investigated in terms of the airfoil requirements for helicopter rotor. To this end, under normal operating conditions of the helicopter rotor, the steady and unsteady aerodynamic characteristics of the Gurney flap are reviewed to reach the following conclusions.

Static Characteristics

The airfoil with the Gurney flap has the zero-lift pitching moment greater than the generally accepted design range but the actual pitching moments considering the dynamic pressure are shown to reside within the design ranges as long as the flap height is kept less than $2\%\ C$. For the modern rotor blade design, the nose-down pitching moment can be partially alleviated by using the reflex airfoil at the inboard region and the blade stall usually starts from the blade tip region. It is appropriate to implement the Gurney flap at the outboard of the rotor blade.

The Gurney flap has little influence on the drag divergence Mach number although zero-lift drag substantially increases when the Gurney flap height is greater than $2\%\ C$.

The drag seems to increase with the Gurney flap height but the performance deterioration due to drag rise is negligible unless its height is greater than 2%. It is worthwhile to note that there exists a critical lift coefficient for which the drag of the Gurney flap airfoil becomes less than that of the baseline airfoil. Thus, for the normal hovering conditions ($M_\infty = 0.6$, $Cl = 0.6$), the drag of the Gurney flap airfoil is smaller than the baseline NACA 0012 airfoil when the flap height is less than $2\%\ C$.

For a given angle of attack, the Gurney flap airfoil has higher drag than the baseline airfoil but the overall lift-to-drag ratios are greatly improved by the Gurney flap as long as the Gurney flap height is kept less than $1\%\ C$. This is because the lift increment is greater than the drag increment. In this sense, it is thought that the implementation of the Gurney flap would greatly improve the figure of merit of the rotor blade in hovering conditions.

After considering the results, it is concluded that there exists some optimum Gurney flap heights, which minimize the drag and pitching moment while maximizing the $Cl_{\max}$ and L/D at the same time. In the present study, the 2% Gurney flap would be a good compromise to satisfy all the major rotorcraft design criteria.

Dynamic Characteristics

It is again confirmed that the numerical computation tends to overpredict the pitching moment and much remains to be done for more accurate numerical simulation. However, the numerical correlation of $Cl_{\max} - Cd_{\max}$ is shown to provide reliable data.

The general dynamic characteristics of the Gurney flap airfoil are similar to those of static ones. It should be noted that no substantial difference in the aerodynamic performance for each airfoil is observed in the deep stall. However, it remains unclear up to this point whether this is due to the limitation of the computation code or not.

In general, the increment of performance improvement increases with the Gurney flap height but the slope is not linear.

The airfoils with the Gurney flap have better aerodynamic performance at the light stall conditions for all Gurney flap heights considered in the present study. Hence, it can be concluded that the Gurney flap is an appropriate device for the application of the rotor blade design.

Acknowledgments

This work was supported by the Korea Research Foundation Grant funded by the Korean Government (MOEHRD) KRF-2005-003-D00058. We also gratefully acknowledge the grant from the Brain Korea 21 Project in 2006. In addition, we would like to acknowledge the support from Korea Institute of Science and Technology Information under The Strategic Supercomputing Support Program. The use of the computing system of the Supercomputing Center is also greatly appreciated.

References

[1] Harris, F. D., "Rotary Wing Aerodynamics: Historical Perspective and Important Issues," *American Helicopter Society National Specialists' Meeting on Aerodynamics and Aeroacoustics*, 1987.

[2] Liebeck, R. H., "Design of Subsonic Airfoils for High Lift," *Journal of Aircraft*, Vol. 15, No. 9, 1978, pp. 547–561.

[3] Neuhart, D. H., and Pendergraft, O. C., Jr., "Water Tunnel Study of Gurney Flaps," NASA TM-4071, Nov. 1988.

[4] Jang, C. S., Ross, J. C., and Cummings, R. M., "Computational Evaluation of an Airfoil with a Gurney Flap," AIAA Paper 92-2708, June 1992.

[5] Storms, B. L., and Jang, C. S., "Lift Enhancement of an Airfoil Using a Gurney Flap and Vortex Generator," *Journal of Aircraft*, Vol. 31, No. 3, 1994, pp. 542–547.

[6] Myose, R., Papadakis, M., and Heron, I., "Gurney Flap Experiments on Airfoils, Wings and Reflection Plane Model," *Journal of Aircraft*, Vol. 35, No. 2, March–April 1998, pp. 206–211.

[7] Van Dam, C. P., Yen, D. T., and Vijgen, P. M. H. W., "Gurney Flap Experiments on Airfoils and Wings," *Journal of Aircraft*, Vol. 36, No. 2, 1999, pp. 484–486.

[8] Giguère, P., Lemay, J., and Dumas, G., "Gurney Flap Effects and Scaling for Low-Speed Airfoils," AIAA Paper 95-1881, June 1995.

[9] Jeffrey, D., Zhang, X., and Hurst, D. W., "Aerodynamics of Gurney Flaps on a Single-Element High-Lift Wing," *Journal of Aircraft*, Vol. 37, No. 2, March–April 2000, pp. 295–301.

[10] Chandrasekhara, M. S., Martin, P. B., and Tung, C., " Compressible Dynamic Stall Performance of a Variable Droop Leading Edge Airfoil with a Gurney Flap," AIAA Paper 2004-41, 2004.

[11] Joo, W., Lee, B. S., Yee, K., and Lee, D. H., "Combining Passive Control Method for Dynamic Stall Control," *Journal of Aircraft*, Vol. 43, No. 4, July–Aug. 2006, pp. 295–301.

[12] Maughmer, M., Lesieutre, G., and Kinzel, M., "Miniature Trailing-Edge Effectors for Rotorcraft Performance Enhancement," *American Helicopter Society 61th Annual Forum*, 2005.

[13] Yeo, H., "Assessment of Active Controls for Rotor Performance Enhancement," *American Helicopter Society 62nd Annual Forum*, 2006.

[14] Lee, B. S., and Lee, D. H., "Data Parallel Symmetric Gauss–Seidel Algorithm for Efficient Distributed Computing," AIAA Paper 97-2138, 1997.

[15] Lee, B. S., "Numerical Study on the Control of Unsteady Separated Flow Fields," Ph.D. Dissertation, Seoul National Univ., Seoul, Republic of Korea, 2005.

[16] Menter, F. R., "Two-Equation Eddy-Viscosity Turbulence Models For Engineering Applications," *AIAA Journal*, Vol. 32, No. 8, 1994, pp. 1598–1605.

[17] McAlister, K. W., Pucci, S. L., McCroskey, W. J., and Carr, L. W., "Experimental Study of Dynamic Stall on Advanced Airfoil Sections Volume 2: Pressure and Force Data," NASA TM 84245, Sept. 1982.

[18] McCroskey, W. J., "Critical Assessment of Wind Tunnel Results for the NACA 0012 Airfoil," NASA TM-100019, Oct. 1987.

[19] Bousman, W. G., "Aerodynamic Characteristics of SC1095 and SC1094 R8 Airfoils," NASA TP-2003-212265, Dec. 2003.

[20] Bousman, W. G., "Evaluation of Airfoil Dynamic Stall Characteristics for Maneuverability," *26th European Rotorcraft Forum*, 2000.
[21] Dadone, L. U., "Design and Analytical Study of a Rotor Airfoil," NASA Contractor Report 2988, May 1978.
[22] Perry, F. J., "Helicopter Rotor Blade," U.S. Patent No. 4427344, filed 13 March 1981.
[23] Bousman, W. G., "Airfoil Design and Rotorcraft Performance," *American Helicopter Society 58th Annual Forum*, 2002.
[24] Smith, M. J., Wong, T., Potsdam, M., Baeder, J., and Phanse, S., "Evaulation of CFD to Determine Two-Dimensional Airfoil Characteristics for Rotorcraft Application," *American Helicopter Society 60th Annual Forum*, 2004.